A numerical study of a pathological example of p-system

Ph. Hoch and M. Rascle.

Laboratoire de Mathématiques, U.R.A. C.N.R.S 168
Université de Nice, Parc Valrose B.P. 71, F06108 Nice Cédex 2

Abstract

In this paper, we consider several high order schemes in one space dimension. In particular, we compare the second order relaxation (ϵ <<1) or "relaxed" (ϵ=0) schemes of Jin-Xin [4], with the second order Lax-Friedrichs scheme of Nessyahu-Tadmor [6], and with higher order ENO and WENO schemes. This comparison is first made on Sod shock tube, and then on a very pathological example of a p-system constructed by Greenberg-Rascle [1]. This exotic system admits a family of periodic solutions which are shock-free but present pairs of *interacting centered compression waves.* Therefore, the exact solution contains big spikes. We show how these different schemes face this numerical challenge.

1 Introduction

The motivation of this paper was to compare several second or higher order schemes -which are precisely described below- on a couple of mono-dimensional problems. The first example is of course the Sod shock tube. The second case is a pathological example of a p-system constructed in [1], see also [2]. This system is built with a very specific pressure law, see the details in Section 2, and admits a family of periodic solutions in space and time. In particular, those solutions are shock-free but present centered compression waves which interact and produce severe spikes. Although this problem is one-dimensional, we have thought it would be interesting to use it as a challenging case to compare several second or higher order finite volume schemes. Namely, we have considered the second order relaxation (ϵ <<1) or relaxed (ϵ=0) schemes of Jin-Xin [4]. We have compared these

schemes on one hand with the staggered second order Lax-Friedrichs scheme of Nessyahu-Tadmor [6], and on the other hand with higher order ENO and WENO schemes, first on Sod's shock tube for Euler equations, and then on this pathological p-system. Not surprisingly, all these schemes work rather well, even in the second case, where the exact solution itself presents big spikes due to the interaction of centered compression waves.
The outline of the paper is as follow. In Section 2, we briefly recall the description of this exotic example constructed in [1]. In Section 3 and 4, we recall a few basic facts, first on higher finite volume schemes and then on second order relaxation schemes. In Section 5, we first compare all these schemes on the more classical -and practically more usefull !- example of Sod's shock tube, and then we present our numerical results and comments on this pathological example, in particular on the presence of spikes, before a brief conclusion in Section 6.

2 A pathological example of p-system

We consider here the p-system, or more exactly the system of one dimensional non linear elasticity in Lagrangian coordinates:

$$\left\{ \begin{array}{l} \partial_t u - \partial_x v = 0, \\ \partial_t v - \partial_x \sigma(u) = 0. \end{array} \right. \tag{1}$$

where u denotes the strain, $\sigma = \sigma(u)$ the stress and v the velocity.
In a very particular case where $\sigma(.)$ is an odd function, Greenberg and Rascle [1] have constructed a sequence of periodic solutions in time and space: $(u^\epsilon, v^\epsilon)(x,t) := (u,v)(\frac{x}{\epsilon}, \frac{t}{\epsilon}), \quad \epsilon \searrow 0$, which satisfies the following properties:
The function u (resp v) is odd (resp even) in x and even (resp odd) in t. Moreover, cf Figure 1, the basic pattern is the interaction of two centered rarefaction waves between two constant states N,S (North,South):

$$N := \left(\begin{array}{c} u = t_0 \\ v = 0 \end{array} \right), \quad S := \left(\begin{array}{c} u = -t_0 \\ v = 0 \end{array} \right), \qquad t_0 > 0,$$

and involve two other constant states E,W (East,West):

$$E := \left(\begin{array}{c} u = 0 \\ v = x_0 \end{array} \right), \quad W := \left(\begin{array}{c} u = 0 \\ v = -x_0 \end{array} \right), \qquad x_0 > 0.$$

In the interior domain of central interaction, the solution is supposed to be the universal solution $(u,v) \equiv (t,x)$.

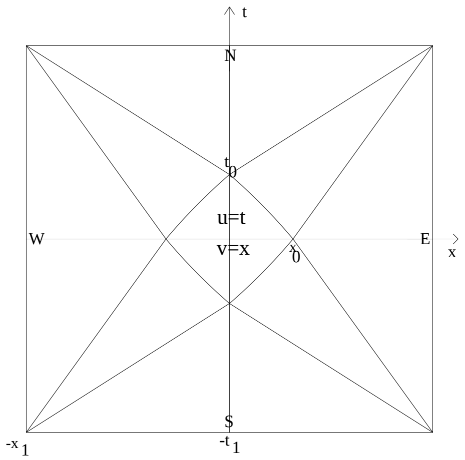

Figure 1

The law is chosen so that the interaction of these two centered rarefaction waves converts them into centered compressive waves, and not in shocks, which would consume energy and would prevent the solution to be periodic in time. In order to obtain this pattern, the constitutive relation σ must satisfy an ODE whose solution writes :

$$\sigma(u) = \frac{c_0^2 \lambda^4}{3} sgn(u) \left(\frac{1}{(\lambda - |u|)^3} - \frac{1}{\lambda^3} \right), \qquad \lambda = t_1 > t_0.$$

In particular, σ is such that :

1. $\forall u \neq 0$, $u\sigma''(u) > 0$, σ: odd. The system is genuinely nonlinear, except for u=0, at which σ presents an inflection point, cf Section 5, Figure 3E.

2. σ is of class C^2, except at u=0, where it is only C^1.

It is important to notice, that if σ were smooth at u=0, then, following Di Perna's result [12], then for all $t > 0$, the initial oscillations of the sequence (u^ϵ, v^ϵ) would be canceled by the nonlinear interactions. Therefore, the sequence (u^ϵ, v^ϵ) considered here is very pathological, since large amplitude oscillations persist, although no eigenvalue is linearly degenerate. In particular, it does not belong to the class of solutions for which Serre [16] [17] constructed formal asymptotic expansions. We have tested a few numerical schemes on this problem with (x,t) $\in (-1,1)^2$, with $x_1 = t_1 = 1$.

The solution consists in 4×4 basic patterns, cf Figure 2 [1].
The initial data (resp boundary conditions on x=-1 and x=+1) on the four successive sub-intervals are NSNS (resp EWEW and EWEW).

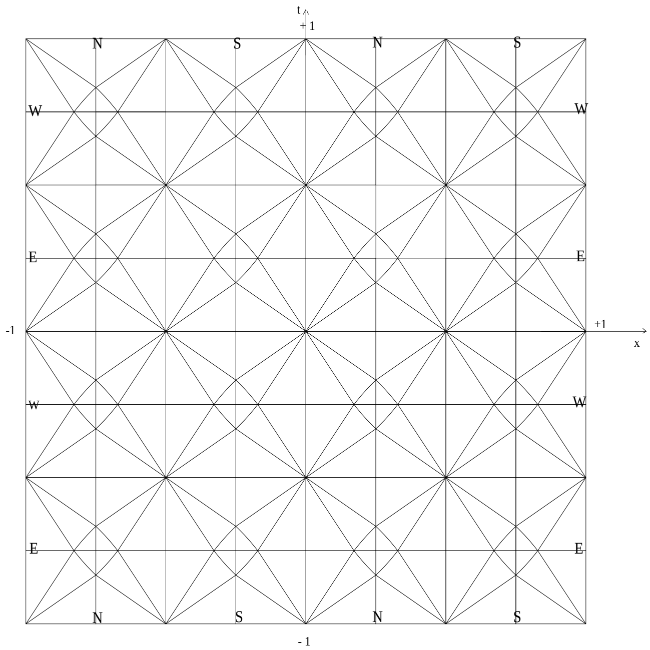

Figure 2

On the numerical point of view, we remark that this solution has no shock, but contains centered rarefaction and compression waves which even interact so that the exact solution presents big spikes, and also that the stress-strain relation σ has an inflection point. These unusual features are therefore a good challenge to test several classical second (or higher) order numerical schemes. Before describing the numerical results in section 5, we first need to describe the schemes we have used.

[1] more exactly, we should consider that a basic pattern is in fact *four* adjacent patterns (see Figure 1), in order to recover the same constant states at the boundary of the period

3 Basic facts on high order finite volume schemes

We consider the initial value problem for a general one dimensional system of N conservation laws:

$$\begin{aligned} \partial_t U + \partial_x F(U) &= 0, && (2)\\ U(x,0) &= U_0(x). && (3) \end{aligned}$$

The system is supposed strictly hyperbolic. We denote by R the matrix of right eigenvectors r_k(U) of F'(U) and we set L:=R^{-1}. We briefly recall the classical construction of high order finite volume schemes:
Let $\bar{U}_j^n$ denote the average value of the numerical solution U(.,t) on the cell $C_j =]x_{j-\frac{1}{2}}, x_{j+\frac{1}{2}}[$ computed at time t^n. Here, we have set $x_j = x_0 + j\Delta x$.
After integration of (2) over the rectangle $C_j \times (t^n, t^{n+1})$, we have to find an approximation of:

$$\bar{U}_j^{n+1} = \bar{U}_j^n - \lambda \left(F_{j+\frac{1}{2}} - F_{j-\frac{1}{2}} \right), \tag{4}$$

where $F_{j+\frac{1}{2}} = \frac{1}{\Delta t} \int_{t^n}^{t^{n+1}} F(U(x_{j+\frac{1}{2}}, t))\, dt, \quad \text{and } \lambda = \Delta t / \Delta x.$
Following Harten [8], we split the algorithm in three steps : reconstruction, evolution, averaging. In the reconstruction step, that we will recall below, we start with the averages $\bar{U}_j^n$, to construct a new function $R(x, \bar{U})$, polynomial on each cell. In the evolution step, we now consider the initial value problem

$$\begin{array}{ll} \partial_t W + \partial_x F(W) = 0, & t \in (t^n, t^{n+1}), \\ W(x, t^n) = R(x, \bar{U}^n). & \end{array} \tag{5}$$

The question is now to approximate the integral:

$$I = \frac{1}{\Delta t} \int_{t^n}^{t^{n+1}} F(W(x_{j+\frac{1}{2}}, t))\, dt,$$

If the function $t \mapsto F(W(x_{j+\frac{1}{2}}, t))$ were known, we would of course use a Gauss type formula of order r:

$$I \simeq \sum_{k=1}^{s} \alpha_k F(W(x_{j+\frac{1}{2}}, t^n + \beta_k \Delta t)) + O(\Delta t^r),$$

For instance, typical choices are:

1. order 1 : s=1, $\alpha_1 = 1$ and $\beta_1 = 0$,

2. order 2 : s=1, $\alpha_1 = 1$ and $\beta_1 = \frac{1}{2}$,

3. order 4 : s=2, $\alpha_1 = \alpha_2 = \frac{1}{2}$, $\beta_1 = \frac{1}{2}(1 - \frac{\sqrt{3}}{3})$, $\beta_2 = \frac{1}{2}(1 + \frac{\sqrt{3}}{3})$.

Now, in order to approximate the above function $F(W((x_{j+\frac{1}{2}}, .)))$, we consider the local Riemann problem:

$$\begin{aligned} &\partial_t Z + \partial_x F(Z) = 0, \\ &Z(x,0) = \begin{cases} a^k_{j+\frac{1}{2}}, \\ b^k_{j+\frac{1}{2}}, \end{cases} \end{aligned} \tag{6}$$

where $a^k_{j+\frac{1}{2}}$ (resp $b^k_{j+\frac{1}{2}}$) is constructed in the following way [8]:
starting from polynomial data $v_j(x)(= R_j(x, \bar{U}))$, in the cell C_j, we first extend this initial data to the neighbor cells. The corresponding solution $v_j(x,t)$ is locally smooth, and $a^k_{j+\frac{1}{2}}$ is the value at point $(x_{j+\frac{1}{2}}, t^n + \beta_k \Delta t)$ of the Taylor expansion of $v_j(x,t)$, denoted by $\tilde{v}_j(x, t^n + t)$, around the point (x_j, t^n), in which we have used the equation to replace all the time derivatives by space derivatives. Of course $b^k_{j+\frac{1}{2}}$ is constructed in a similar way in the cell C_{j+1}, therefore for i=j,j+1 and r=3:

$$a^k_{j+\frac{1}{2}} = \tilde{v}_j(x_{j+\frac{1}{2}}, t^n + \beta_k \Delta t) \text{ and } b^k_{j+\frac{1}{2}} = \tilde{v}_{j+1}(x_{j+\frac{1}{2}}, t^n + \beta_k \Delta t)$$

$$\tilde{v}_i(x, t^n + t) = \tilde{v}_i(x, t^n) - t\partial_x f(\tilde{v}_i(x, t^n)) + \frac{t^2}{2}\partial_x(f'(\tilde{v}_i(x, t^n))\partial_x f(\tilde{v}_i(x, t^n)))$$

With $\tilde{v}_i(x, t^n) = v_i(x, 0) = R(x, \bar{u})_{|C_i}$.

Therefore, with the proprerty on $R(x, \bar{u})$:

$$\frac{\mathrm{d}^k}{\mathrm{d}x^k} R_i(x, \bar{u}^n) = \frac{\partial^k}{\partial x^k} u(x, t^n + t) + O(\Delta x^{r-k}) \qquad 0 \le k \le r-1.$$

We have : $\quad \tilde{v}_i(x, t^n + t) = u(x, t^n + t) + O(\Delta x^r) \quad$ when $\Delta x = O(\Delta t)$.

Therefore, the exact flux of the solution to the Riemann Problem (6) satisfies :
$f^G(a,b) = f(Z^R(0,a,b)) = f(u(x_{j+\frac{1}{2}}, t^n + t)) + O(\Delta x^r)$,
where f^G means the Godunov flux. Practically we may take any numerical flux g(a,b) which is Lipschitz continuous and monotone. Here, we will use the Roe scheme with the entropy fix used by Osher-Shu see [10]. The averaging is obtain by taking the average value of the solution $U(x, t^{n+1})$ on

the cell C_j. Finally, the scheme writes:

$$\bar{U}_j^{n+1} = \bar{U}_j^n - \lambda \left(\sum_{k=1}^{s} \alpha_k (g(a^k_{j+\frac{1}{2}}, b^k_{j+\frac{1}{2}}) - g(a^k_{j-\frac{1}{2}}, b^k_{j-\frac{1}{2}})) \right) \tag{7}$$

Of course, the Godunov and Van Leer MUSCL schemes belong to this class, as well as the ENO schemes, and also the (second) order staggered Lax-Friedrichs scheme of Nessyahu-Tadmor [6], provided that we average at each time step on the staggered grid. Of course that avoids using any Riemann solver. This scheme can also be viewed as a predictor-corrector scheme:

$$\bar{U}_j^{n+\frac{1}{2}} = \bar{U}_j^n - \frac{\lambda}{2} F_j'^n, \tag{8}$$

$$\bar{U}_{j+\frac{1}{2}}^{n+1} = \frac{1}{2}(\bar{U}_j^n + \bar{U}_{j+1}^n) - \frac{1}{8}(U_{j+1}'^n - U_j'^n) - \lambda \left(F(\bar{U}_{j+1}^{n+\frac{1}{2}}) - F(\bar{U}_j^{n+\frac{1}{2}}) \right). \tag{9}$$

Where $F_j'^n/\Delta x$ and $U_j'^n/\Delta x$ are numerical approximation of resp. $\partial_x F(U(x_j, t^n))$ and $\partial_x U(x_j, t^n)$.
Now, if Δt goes to zero in (7), we obtain:

$$\frac{\mathrm{d}}{\mathrm{d}t}\bar{U}_j(t) = -\frac{1}{\Delta x} \left(g(R_j(x_{j+\frac{1}{2}}, \bar{U}), R_{j+1}(x_{j+\frac{1}{2}}, \bar{U})) - g(R_{j-1}(x_{j-\frac{1}{2}}, \bar{U}), R_j(x_{j-\frac{1}{2}}, \bar{U})) \right) \tag{10}$$

which allows to uncouple spatial and temporal approximation.
Now, (10) is a system of ODE that we approach with the Runge-Kutta Total Variation Diminishing (TVD) method of Osher, Shu [9] p(444-447).
As observed in [10], the WENO reconstruction allows to gain one order of accuracy at the interfaces. Therefore, the time approximation must be of order (r+1) to exploit this gain.
We now briefly recall the reconstruction procedure. Starting with known averages $\bar{U}_j^n$ on each cell C_j, we construct a piecewise polynomial function $R(x, \bar{U})$ which satisfies the following properties:

(i) High order approximation in regions where the solution is smooth: $R_j(x, \bar{U}) = U(x, t) + e(x)\Delta x^r + O(\Delta x^{r+1})$.

(ii) Conservation of average values : $\bar{R}(x_j, \bar{U}) = \bar{U}_j$.

(iii) Control of oscillations, either TVD no oscillation is created : $TV(R(x, \bar{u})) \leq TV(u)$ or ENO : $TV(R(x, \bar{u})) \leq TV(u) + O(\Delta x^r)$.

We begin with the scalar case, the construction is based on the primitive of u(.,t) [2]:

$$W(x) = \int_{x_{j_0-\frac{1}{2}}}^{x} u(y,t)\, dy,$$

with $W(x_{j+\frac{1}{2}}) = \Delta x \sum_{k=j_0}^{j} \bar{u}_k$. Knowing the values of W at the interfaces provides an approximation of u by evaluating the derivatives of a polynomial interpolation of W at the interfaces. Let us simply recall that we typically obtain:

(i) for r=1, the Godunov scheme: $R_j(x, \bar{u}) = \bar{u}_j$

(ii) for r=2, Van leer's type of schemes: $R_j(x, \bar{u}) = \bar{u}_j + \frac{\sigma_j}{\Delta x}(x - x_j)$, where $\sigma_j = \Delta x \partial_x u(x_j, t) + O(\Delta x^2)$ if TVD, or $\sigma_j = \Delta x \partial_x u(x_j, t) + O(\Delta x^3)$ if UNO (see [7]).

(iii) for $r > 2$, either the ENO or the WENO type of schemes. The latter involves a convex combination of *all* the interpolation polynomials of W on the stencil $S_{j+k} = (x_{j+k-r+\frac{1}{2}}, ..., x_{j+k+\frac{1}{2}})$, whereas the former only involves *one* of them.

Finally, in the case of systems considered here, the reconstruction has been performed either component wise, e.g in LF2 or in characteristic variables (ENO, WENO). In the next section, we recall the construction of relaxation schemes [4].

4 Second order relaxation schemes

The basic idea of relaxation schemes [4] is to (formally) consider a nonlinear hyperbolic system of conservation laws

$$\partial_t U + \partial_x F(U) = 0, \tag{11}$$

as the zero-relaxation limit, of a sequence of semi-linear hyperbolic systems of size 2N, with a stiff source term:

$$\begin{aligned} \partial_t U + \partial_x V &= 0, && (12) \\ \partial_t V + A^2 \partial_x U &= \frac{1}{\epsilon}(F(U) - V),\ \epsilon \searrow 0 && (13) \end{aligned}$$

[2]Called reconstruction via primitive function

Here A^2 is a constant diagonalizable matrix (practically, A is diagonal), and we assume that the classical subcharacteristic condition of Whitham [15], Liu [13], is satisfied, namely that the characteristic speeds of the full system (12) (13) "dominate" those of the relaxed equilibrium system (11) : $A^2 \geq F'(U)^2$, see a more precise statement in [14]. Let (U,V):=(U^ϵ, V^ϵ) be the solution to (12)(13). If we consider the Chapman-Enskog expansion:
$V^\epsilon = V_0(U) + \epsilon V_1(U, \partial_x U) + ...,$
where U is the solution to the equilibrium system, then we classically obtain, see e.g [18]:

$$V_0(U) = F(U^\epsilon),$$

and finally, at the order ϵ, U^ϵ satisfies:

$$\partial_t U^\epsilon + \partial_x F(U^\epsilon) = \epsilon \partial_x ((A^2 - F'(U^\epsilon)^2) \partial_x U^\epsilon) \tag{14}$$

which is well posed, in view of the sub-characteristic condition. There are essentially two classes of schemes introduced in [4]. In either case, the scheme is based on the obvious splitting between the stiff ODE:

$$\begin{cases} \partial_t U = 0, \\ \partial_t V = \frac{1}{\epsilon}(F(U) - V), \end{cases} \tag{15}$$

and the conservation law without source term:

$$\begin{cases} \partial_t U + \partial_x V = 0, \\ \partial_t V + A^2 \partial_x U = 0. \end{cases} \tag{16}$$

The stiff ODE (15) is either approximated with an implicit (not A-stable) second order Runge-Kutta method, or replaced by the equilibrium relation

$$V := F(U). \tag{17}$$

The latter choice is much more natural as soon as the time step satisfies:

$$\Delta t / \epsilon >> 1, \tag{18}$$

which is the practical case. As in [4], in order to approximate the convective part (16), we use here the MUSCL reconstruction, based on the Riemann invariants. We consider here the case where: A = c I, $c > 0$, where I is the unit 2×2 matrix. The corresponding vector-valued Riemann invariants are the linear functions:

$$W = V + AU, \quad Z = V - AU, \;\; W, Z \in I\!R^2, \tag{19}$$

and the sub-characteristic condition is simply:

$$c^2 \geq \sigma'(u). \tag{20}$$

Taking into account the associate characteristic speeds, the corresponding reconstructions are:

$$R_j^+(x_{j+\frac{1}{2}}, \bar{W}) = \bar{W}_j + \frac{\sigma_j^+}{2},$$
$$R_j^-(x_{j-\frac{1}{2}}, \bar{Z}) = \bar{Z}_j - \frac{\sigma_j^-}{2},$$

where $\sigma_j^+ = \partial_x W(x_j, .)\Delta x + O(\Delta x^2)$,
and $\sigma_j^- = \partial_x Z(x_j, .)\Delta x + O(\Delta x^2)$, are obtained with the Van-Leer slope limiter [3], Using (19) to recover the original variables, we obtain the numerical fluxes:

$$G_{j+\frac{1}{2}}(U) = \frac{1}{2c}(R_j^+(x_{j+\frac{1}{2}}, \bar{V} + A\bar{U}) - R_{j+1}^-(x_{j+\frac{1}{2}}, \bar{V} - A\bar{U})),$$
$$G_{j+\frac{1}{2}}(V) = \frac{1}{2}(R_j^+(x_{j+\frac{1}{2}}, \bar{V} + A\bar{U}) + R_{j+1}^-(x_{j+\frac{1}{2}}, \bar{V} - A\bar{U})).$$

Finally, the MUSCL scheme used here combines this spatial approximation with a second order Runge-Kutta method [9], which is TVD, provided that the CFL condition 1/2 is satisfied. Now, we can describe the full relaxation schemes used here. In the first case, we solve numerically the stiff ODE, with the above-mentioned implicit second order Runge-Kutta method [4], see also [5], to obtain the relaxation (called relaxing in [4]) scheme:

$$\left\{ \begin{array}{l} \bar{U}_j^{n+\frac{1}{4}} = \bar{U}_j^n, \\ \bar{V}_j^{n+\frac{1}{4}} = \bar{V}_j^n - \frac{\Delta t}{\epsilon}(F(\bar{U}_j^{n+\frac{1}{4}}) - \bar{V}_j^{n+\frac{1}{4}}), \end{array} \right. \tag{21}$$

$$\left\{ \begin{array}{l} \bar{U}_j^{n+\frac{2}{4}} = \bar{U}_j^{n+\frac{1}{4}} - \Delta t D_j^{conv} V^{n+\frac{1}{4}}, \\ \bar{V}_j^{n+\frac{2}{4}} = \bar{V}_j^{n+\frac{1}{4}} - \Delta t A^2 D_j^{conv} U^{n+\frac{1}{4}}, \end{array} \right. \tag{22}$$

$$\left\{ \begin{array}{l} \bar{U}_j^{n+\frac{3}{4}} = \bar{U}_j^{n+\frac{2}{4}}, \\ \bar{V}_j^{n+\frac{3}{4}} = \bar{V}_j^{n+\frac{2}{4}} + \frac{2\Delta t}{\epsilon}(F(\bar{U}_j^{n+\frac{1}{4}}) - \bar{V}_j^{n+\frac{1}{4}}) + \frac{\Delta t}{\epsilon}(F(\bar{U}_j^{n+\frac{3}{4}}) - \bar{V}_j^{n+\frac{3}{4}}), \end{array} \right. \tag{23}$$

$$\begin{cases} \bar{U}_j^{n+\frac{4}{4}} = \bar{U}_j^{n+\frac{3}{4}} - \Delta t D_j^{conv} V^{n+\frac{3}{4}}, \\ \bar{V}_j^{n+\frac{4}{4}} = \bar{V}_j^{n+\frac{3}{4}} - \Delta t A^2 D_j^{conv} U^{n+\frac{3}{4}}, \end{cases} \tag{24}$$

$$\begin{cases} \bar{U}_j^{n+1} = \frac{1}{2}(\bar{U}_j^{n+\frac{4}{4}} + \bar{U}_j^n), \\ \bar{V}_j^{n+1} = \frac{1}{2}(\bar{V}_j^{n+\frac{4}{4}} + \bar{V}_j^n). \end{cases} \tag{25}$$

In the second case, we just replace steps (21) (resp (23)) by imposing the equilibrium relation (26) (resp (27)):

$$\bar{V}_j^{n+\frac{1}{4}} = F(\bar{U}_j^{n+\frac{1}{4}}), \tag{26}$$

$$\bar{V}_j^{n+\frac{3}{4}} = F(\bar{U}_j^{n+\frac{3}{4}}). \tag{27}$$

The resulting scheme (26) (22) (27) (24) (25) is called the *zero-relaxation scheme* [3]. In the case of (1), where U=(u,v), we have also considered a physically more natural relaxation system:

$$\begin{cases} \partial_t u - \partial_x v = 0, \\ \partial_t v - \partial_x (c^2 u + Y) = 0, \\ \partial_t Y = \frac{1}{\epsilon}(\sigma(u) - c^2 u - Y). \end{cases} \tag{28}$$

The adaptation to this case is straightforward. We just note that the sub-characteristic condition is still:

$$c^2 \geq \sigma'(u). \tag{29}$$

Remark

As it is well known, if we approximate the convective part (16) by the upwind scheme with a CFL=1 and impose the equilibrium in (15) for the 4×4 system, then we just recover the Lax-Friedrichs scheme for the equilibrium system (11). We note that the three eigenvalues of (28), are: -c, 0, c, and therefore are interlaced with those of (1) in the sense of Chen, Levermore, Liu [14].

[3] also called *relaxed scheme* in [4]

5 Numerical results

Before describing the results for the special p-system (1), we have first considered the test-case of Sod shock tube for one dimensional compressible Euler equations:

$$\begin{cases} \partial_t \rho + \partial_x m = 0, \\ \partial_t m + \partial_x(\frac{m^2}{\rho} + p) = 0, \\ \partial_t E + \partial_x(\frac{m}{\rho}(E+p)) = 0. \end{cases} \tag{30}$$

$$p = (\gamma - 1)(E - \frac{1}{2}\frac{m^2}{\rho}) \qquad \gamma = 1.4$$

5.1 The case of Sod's shock tube

On this problem, we have tested several schemes:

(i) the second order staggered Lax-Friedrichs scheme (8) (9) (plotted with $+$), and the zero-relaxation scheme (26) (22) (27) (24) (25) (plotted with $\times$), see Figures (1A 2A 3A).

(ii) the relaxation scheme (21) (22) (22) (24) (25) with $\epsilon = 10^{-4}$ (plotted with $+$) and 10^{-8} (plotted with $\times$), see Figures (1B 2B 3B).

The reference solution (plain line) has been obtained with the fourth order WENO scheme with $\Delta x = .00025$. The numerical solution displayed with ($+$) or ($\times$) is computed at time t=.1644, the space and time steps are $\Delta x = .0025$, $\Delta t = .0005565$ and the Riemann data are: $(\rho, m, E)^- = (1, 0, 2.5)$, $(\rho, m, E)^+ = (.125, 0, .25)$.
We have compared more precisely these schemes. In Figures 1C, 2C, 3C, we have simultaneously plotted the *differences* between the reference solution and:

1. (i) LF2 plotted with ($+$),
2. (ii) the zero-relaxation plotted with ($\times$).

In the same way, Figures 1D, 2D and 3D show the *differences* between the zero-relaxation and :

1. (i) the $\epsilon = 10^{-4}$ case plotted with ($+$),
2. (ii) the $\epsilon = 10^{-8}$ case plotted with ($\times$).

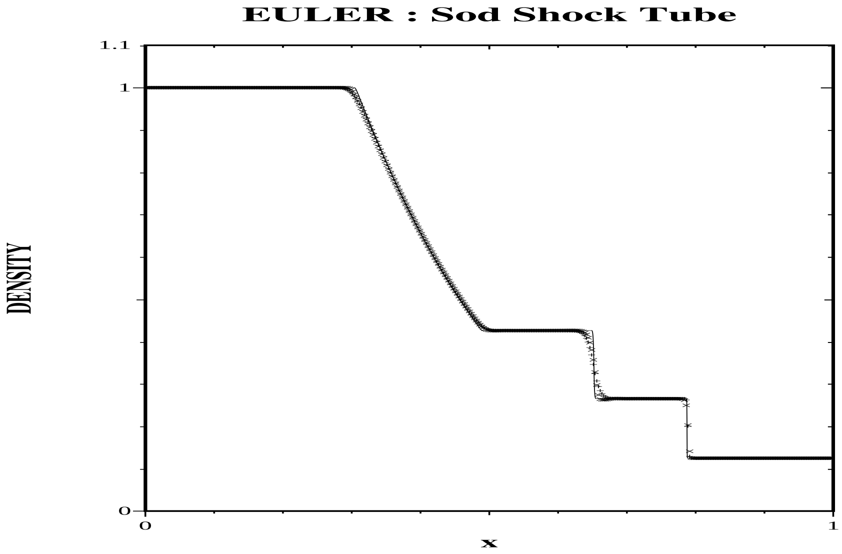

Figure 1A

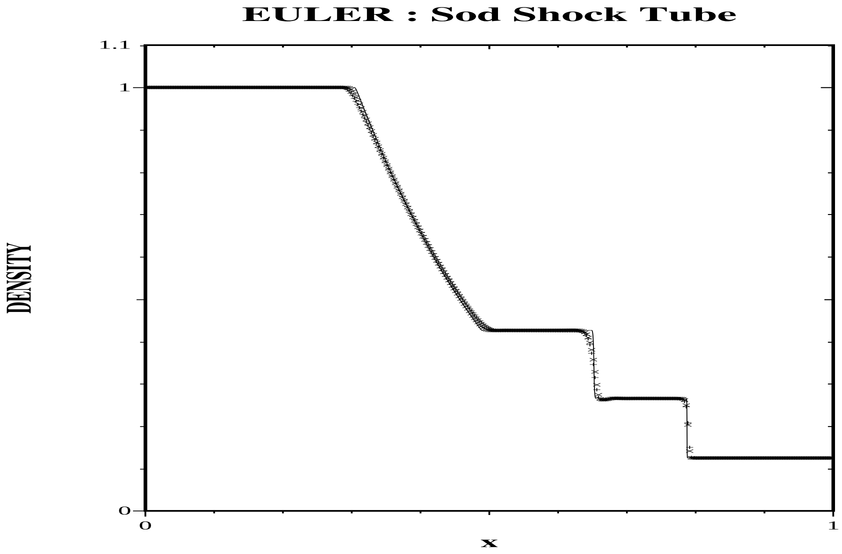

Figure 1B

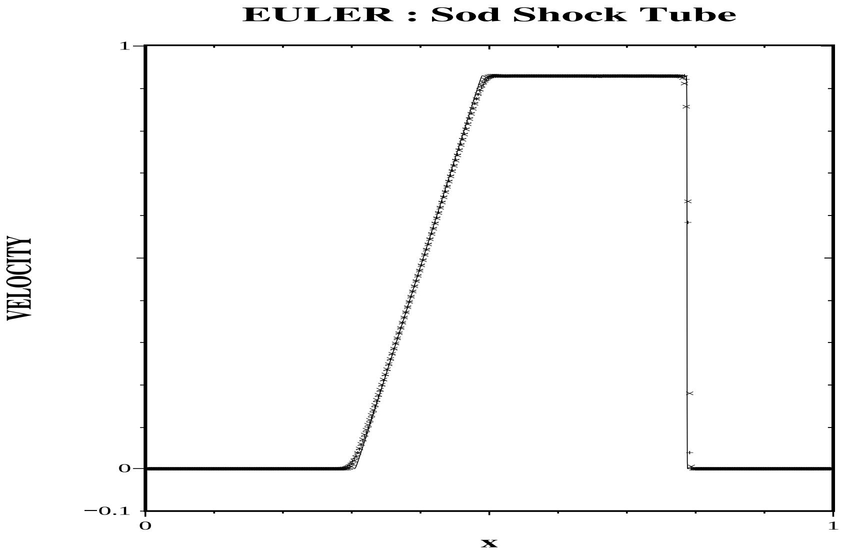

Figure 2A

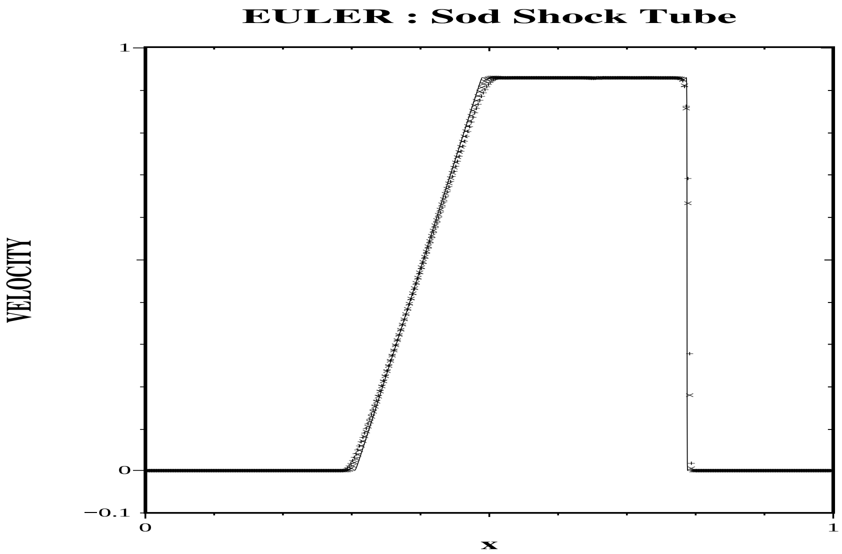

Figure 2B

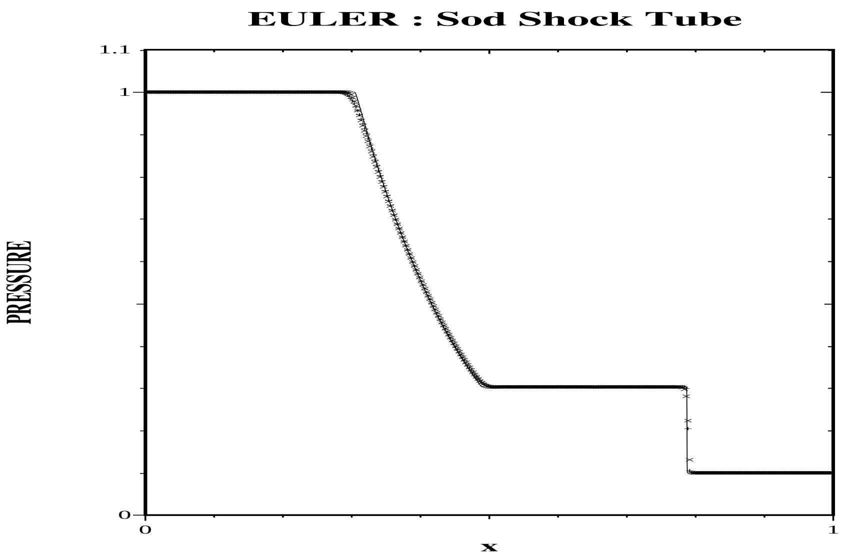

Figure 3A

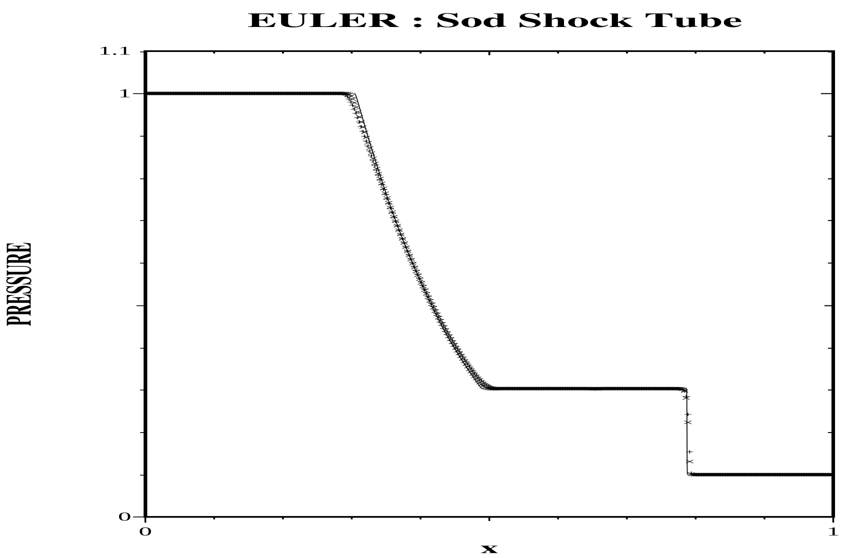

Figure 3B

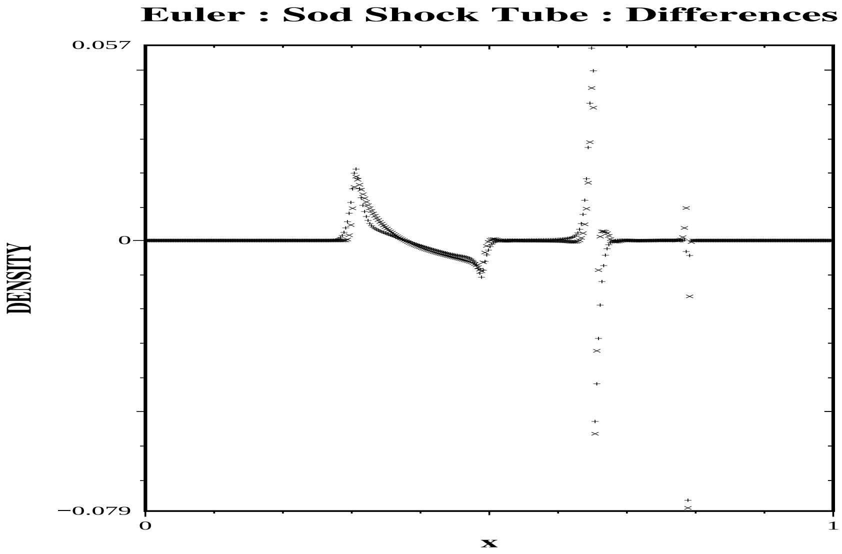

Figure 1C

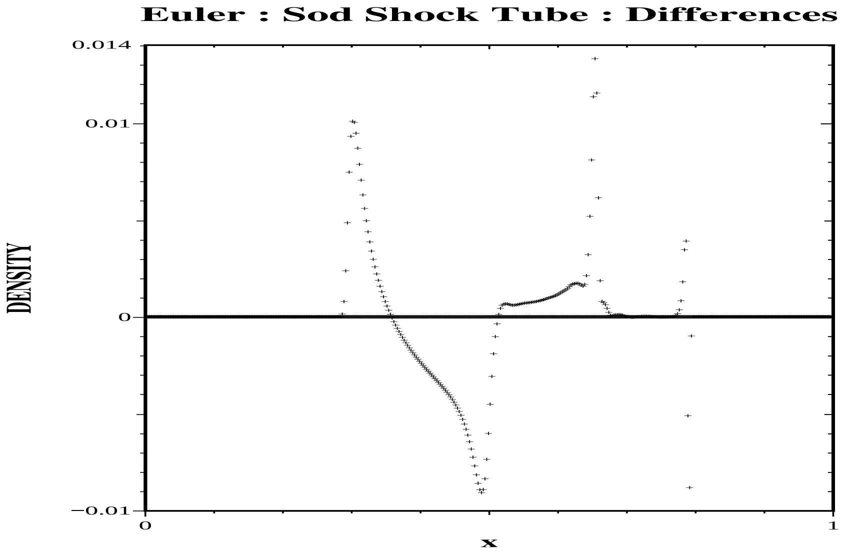

Figure 1D

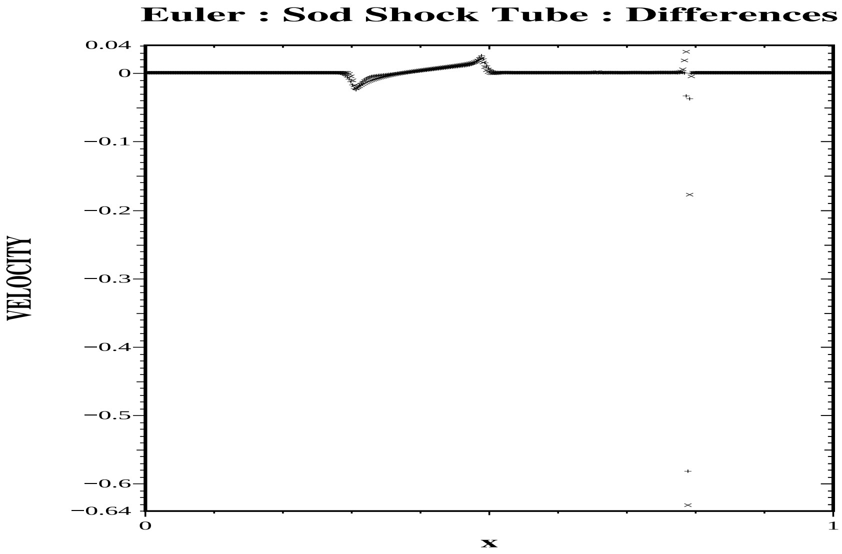

Figure 2C

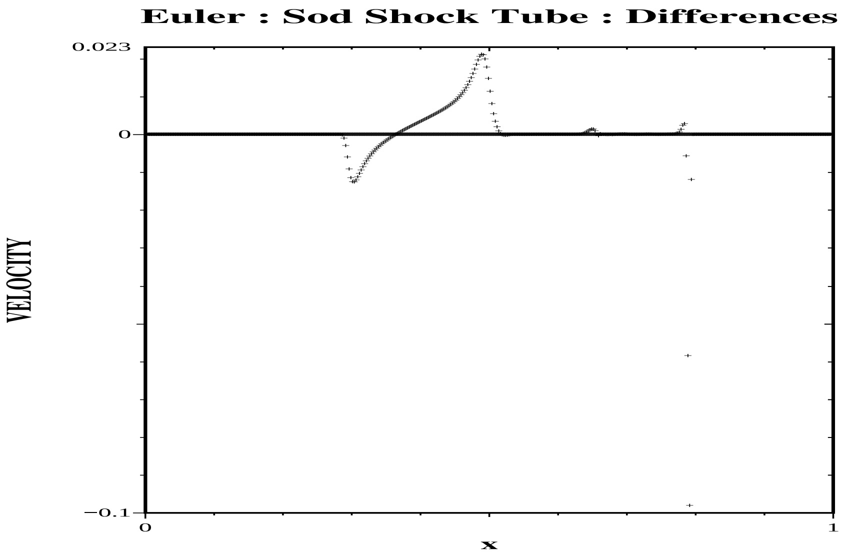

Figure 2D

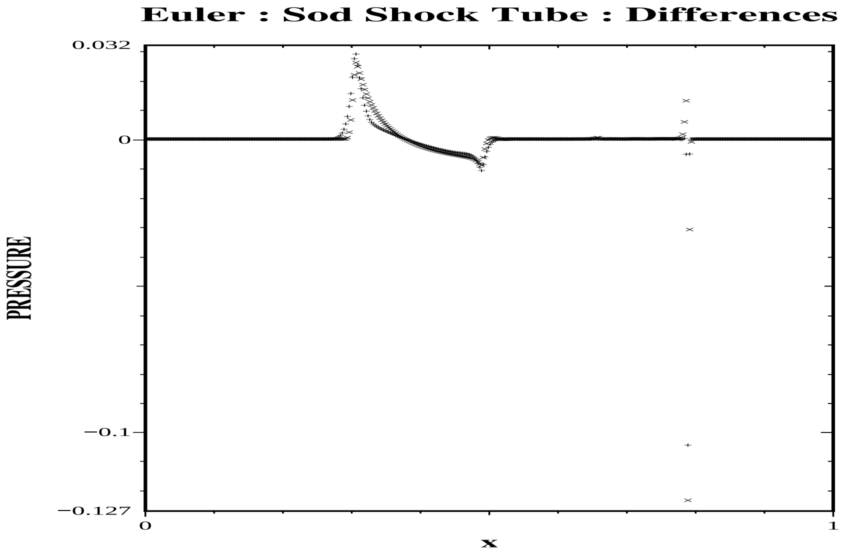

Figure 3C

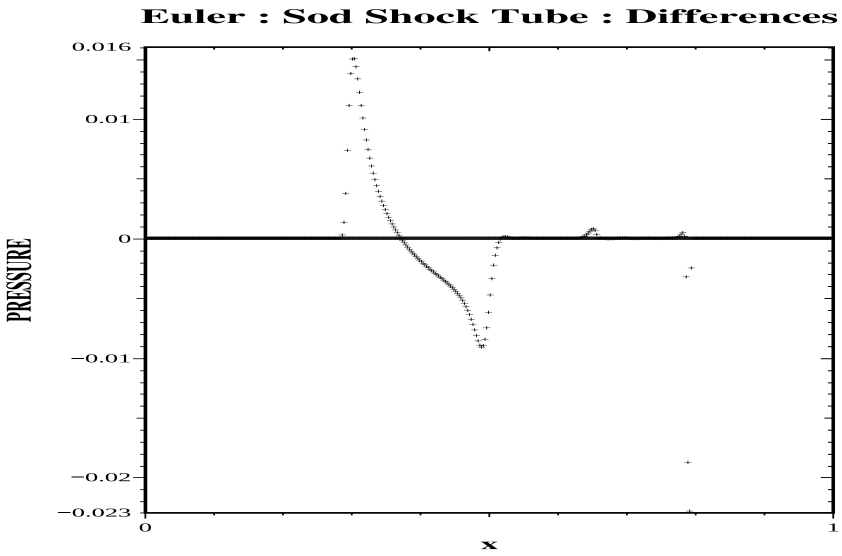

Figure 3D

Comments:

1. The relaxation ("relaxing") and the zero-relaxation ("relaxed") schemes have been tested in [4] with the same matrix A^2, with a CFL=0.75 and $\Delta x = 0.005$, instead of CFL=0.5 and $\Delta x = 0.0025$ here, which may explain why our numerical results are nicer.

2. All these schemes studied here give comparable results. We see in Figures (1,2,3) A and C, that LF2 scheme produces a slightly sharper shock than the zero-relaxation (one grid point instead of three), but on the contrary the contact discontinuity and the rarefaction wave are slightly more spread out.

3. Not surprisingly, in Figures (1,2,3) B and D, the results of the zero-relaxation scheme are almost exactly the same -up to 10^{-6}- as in the case ϵ=10^{-8}. In fact, the curves are undistinguishable. On the other hand the waves are (slightly) more spread out in the ϵ=10^{-4} case, with a maximal difference of 10^{-2} with the zero-relaxation case. We recall that $\Delta t \simeq 5.6\ 10^{-4}$, so that in this case $\Delta t/\epsilon = 5.6 = O(1)$. In all cases the maximal difference is reached at the shock, or at the contact discontinuity (except of course for the velocity and the pressure) but is also not negligible at the edges of the rarefaction wave (see Figures (1,2,3) C and D).

4. In the sequel, we will only compare the zero-relaxation and the second order staggered Lax-Friedrichs scheme with the other high order schemes.

5.2 The special p-system

We have considered the case where the parameters given in section 2 are : $c_0 = 0.75$, $u_0 = 0.25$, $x_0 = 0.25$,$\lambda = 1$, $x_1 = 1$, $t_1 = 1$.
The initial data are alternately N:=(u_0,0) and S:=(-u_0,0). The space and time steps are $\Delta x = 2\,10^{-3}$ and $\Delta t = 5\,10^{-4}$, the CFL condition is 1/3. The solution therefore consists of 4×4 basic patterns.
We have considered:

(i) the second order zero-relaxation scheme (26) (22) (27) (24) (25), either for the 4×4 system (12) (13), see Figures 4A, 4B, or for the physically more natural 3×3 system (28), see Figures 5A, 5B.

(ii) the second order staggered Lax-Friedrichs scheme (8) (9), either with the TVD, see Figures 6A, 6B, or with the UNO reconstruction, see Figures 7A, 7B.

(iii) the ENO schemes (7) of order 2 see Figures 8A, 8B, or 4, see Figures 9A, 9B.

(iv) the WENO schemes of order 3 see Figures 10A, 10B, or 4, see Figures 11A, 11B.

In all the pictures, the results are displayed at final time t=1. We have also displayed in Figures 13 (A,B) and 14 (A,B), the numerical results -only with the second order zero-relaxation scheme- at time t=0.75, which corresponds to u=0, which is the inflection point of the strain-stress relation $\sigma(u)$, see Figure 3E:

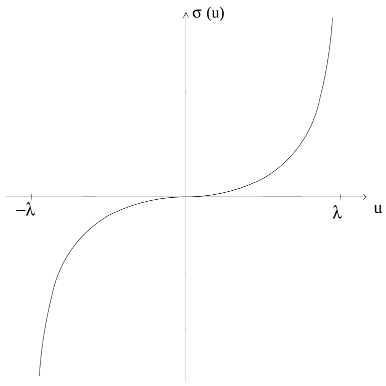

Figure 3E

zero-relaxation schemes

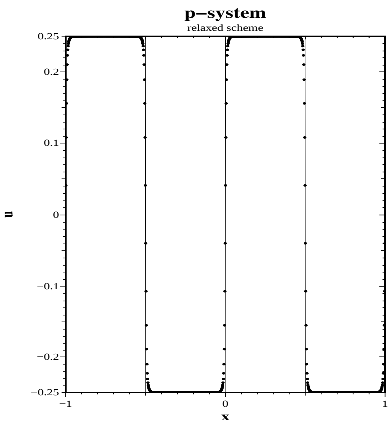

Figure 4A

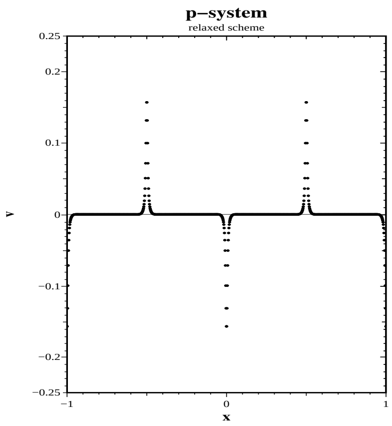

Figure 4B

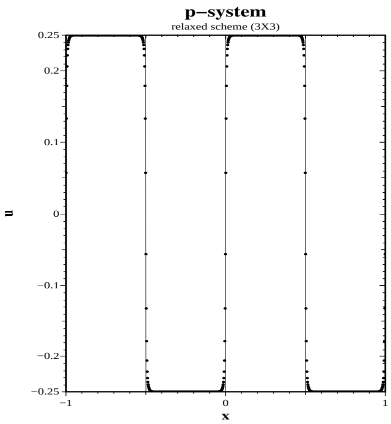

Figure 5A

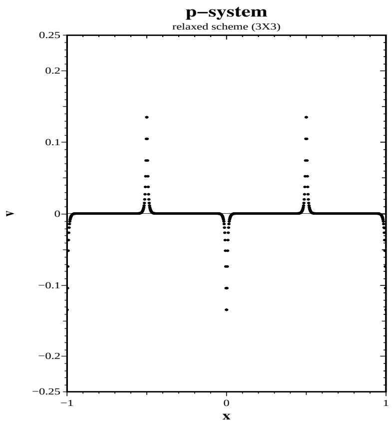

Figure 5B

Staggered Lax-Friedrichs

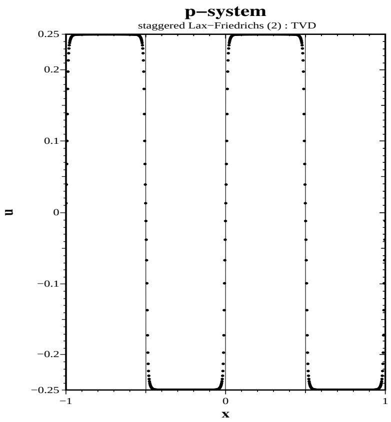

Figure 6A

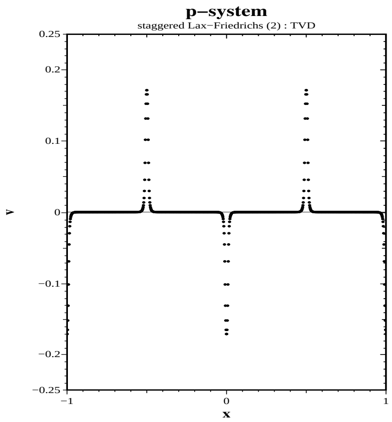

Figure 6B

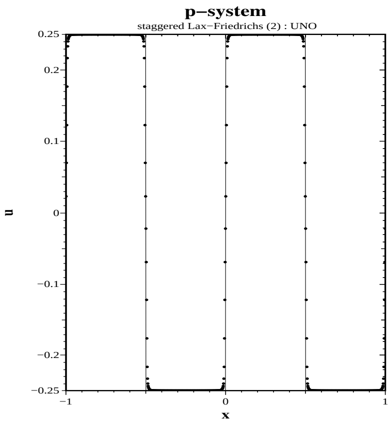

Figure 7A

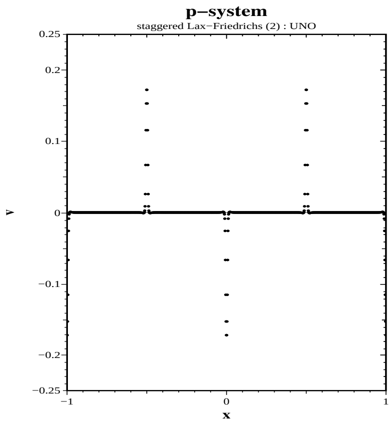

Figure 7B

ENO schemes

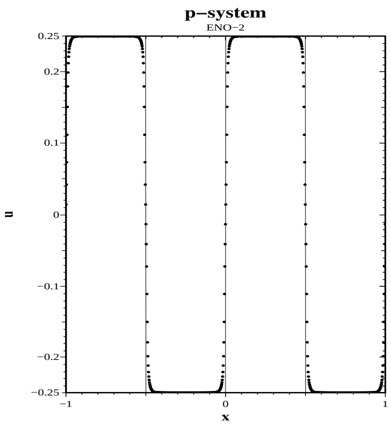

Figure 8A

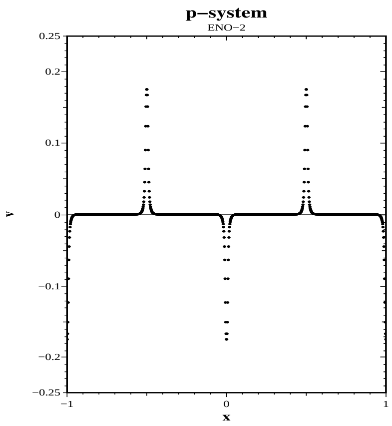

Figure 8B

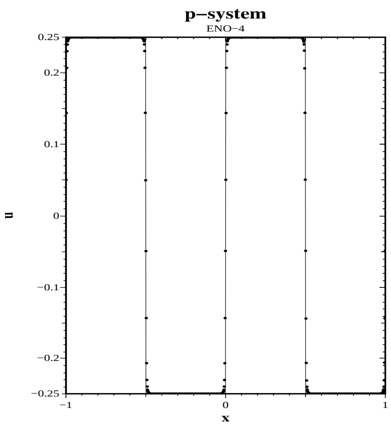

Figure 9A

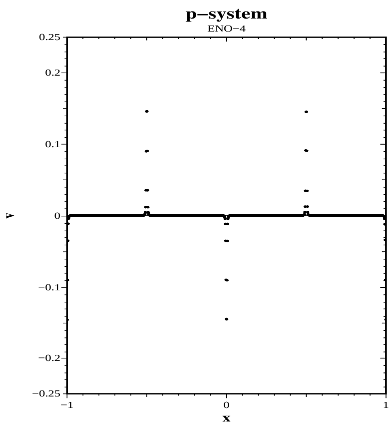

Figure 9B

WENO schemes

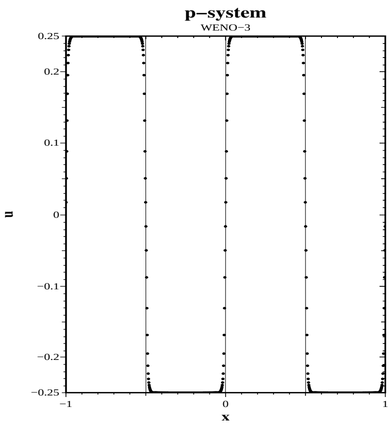

Figure 10A

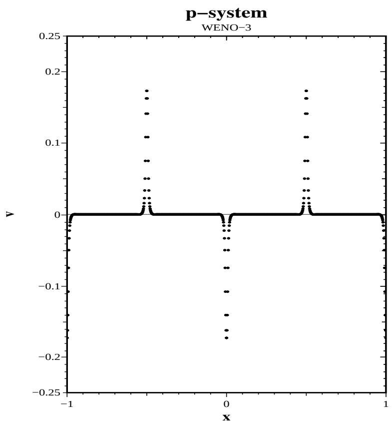

Figure 10B

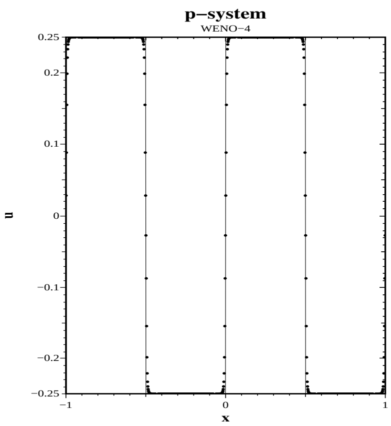

Figure 11A

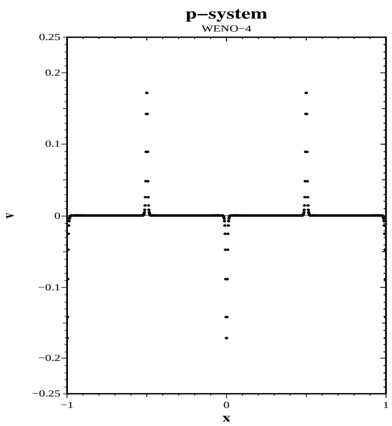

Figure 11B

Comments

All the schemes are comparable and give quite good results, apart from the numerical spikes. Those numerical spikes only involve the velocity v and the bigest ones are located near by the centers of interacting compression waves, but there are also smaller ones at the inflection point u=0, e.g at t=0.75, see Figure 13 A.

We have first thought that this phenomenon was similar to the spikes produced by (first order) Lax-Friedrichs scheme near by a slowly moving shock [11]. In fact, this is not the case. The reason for those spikes is double. First, the exact solution itself presents big spikes in v, except *exactly* at time t=1, see Figure 2, and next, that the numerical propagation speed is slightly smaller than the exact one. Therefore, the numerical solution depicted for instance in Figure 5A, 5B would be a better approximation of the exact solution at some time $t^* = 1 - O(\Delta t)$. Similarly, for instance, with the zero-relaxation scheme, the numerical results at time t=1+7 Δt are much better, see Figures 12 A,B. The same phenomenon occurs near by the inflection point at time t=0.75 + 6 Δt, see Figure 14A (we recall that $\Delta t = 5\,10^{-4}$).

Numerical solution at time t=1+7 Δt

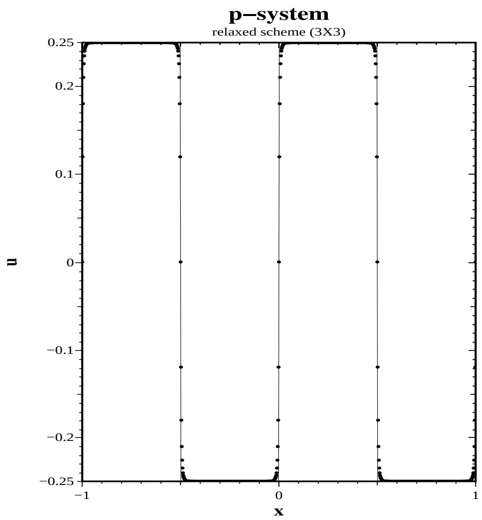

Figure 12A

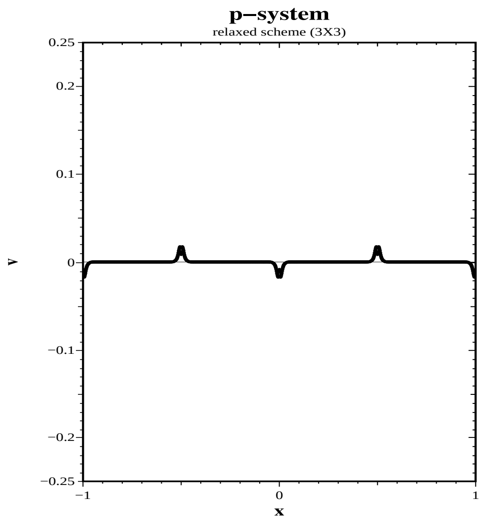

Figure 12B

Numerical solution at inflection point t=0.75

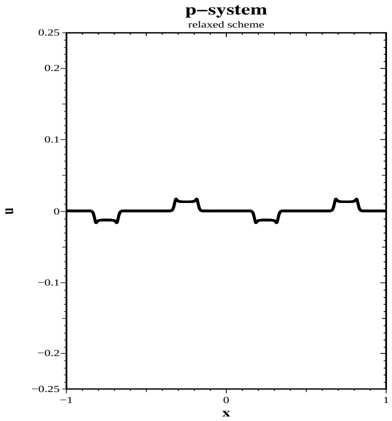

Figure 13A

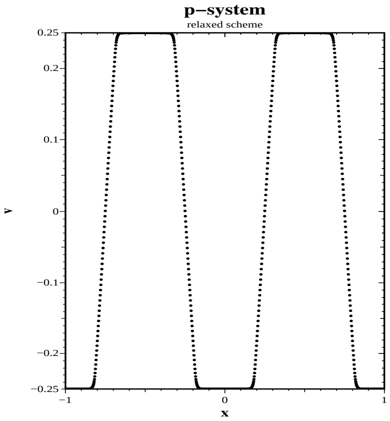

Figure 13B

Numerical solution at t=0.75 + 6 Δt

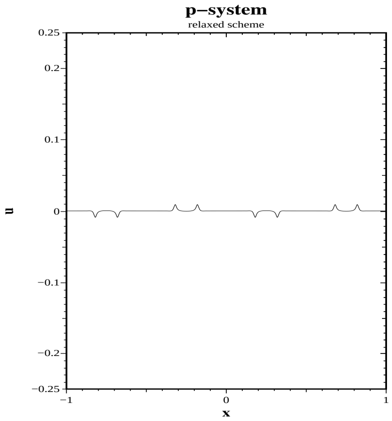

Figure 14A

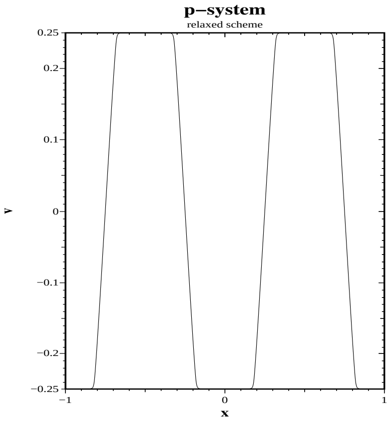

Figure 14B

6 Conclusion

In this paper, we have considered and compared several classes of high order finite volume schemes, first on Sod's shock tube for compressible Euler equations, and then on a one dimensional pathological example, where even the exact solution contains severe spikes, due to the interaction of centered compression waves. All these schemes give comparable results and work rather well, considering the stiffness of the problem. The numerical spikes are essentially due to the fact that the numerical propagation speed is slighty smaller than the exact one, so that the numerical solution "is late". If the problem were linear, a classical Fourier analysis would probably explain this phenomenon.

References

[1] J.M. Greenberg, M. Rascle , "Time-periodic solutions to systems of conservation laws ", Arch. Ration. Mech. Anal. (115), No.4, 395-407, (1991).

[2] J.M. Greenberg, R. Peszek ,"Time periodic solutions to a class of quasilinear wave equations", Arch. Ration. Mech. Anal. (122), No.1, 35-51, (1993).

[3] P.K. Sweby, High Resolution schemes using flux limiters for hyperbolic conservation laws, SIAM J. Num. Anal. (21), 995-1006, (1984).

[4] S. Jin, Z. Xin, "The Relaxing schemes for systems of conservation laws in arbitrary space dimensions", Comm. Pure. Appl. Math. (48), 235-277, (1995).

[5] R. Caflish, S. Jin, G. Russo ,"Uniformly accurate schemes for hyperbolic systems with relaxation", SIAM J. Num. Anal. (34), 246-281, (1997).

[6] H. Nessyahu, E. Tadmor, "Non-oscillatory central differencing for hyperbolic conservation laws", J. Comp. Phys. (87), N^o2., 408-463, (1990).

[7] A. Harten, S. Osher, "Uniformly high order accurate nonoscillatory schemes. I". SIAM J. Numer. Anal. (24), 279-309 (1987).

[8] A. Harten, S. Osher, B. Engquist, L. Chakravarthy, "Uniformly high order accurate essentially non-oscillatory schemes, III", J. Comp. Phys. (71), 231-303, (1987).

[9] S. Osher, C.W. Shu, "Efficient implementation of ENO schemes, I", J. Comput. Phys. (77), No.2, 439-471 (1988).

[10] X.D Liu, S. Osher, T. Chan, "Weighted essentially non-oscillatory schemes", J. Comput Physics. (115), 200-212, (1994).

[11] S. Jin, J-G Liu, "The behavior of numerical schemes near slowly moving shocks", Preprint.

[12] R. Di Perna, "Convergence of approximate solutions to conservation laws", Arch. Ration. Mech. Anal., (82), 27-70, (1983).

[13] T.P. Liu, "Hyperbolic conservation laws with relaxation", Comm. Math. Phys. (108), 153-175, (1987).

[14] G.Q Chen, C.D Levermore, T.P Liu, "Hyperbolic conservation laws with stiff relaxation terms and entropy", Comm. Pure Appl. Math. (47), 787-830, (1994).

[15] G.B Whitham, "Linear and non Linear Waves", New York, John Wiley and Sons, 1974.

[16] D. Serre, "Oscillations non lineaires des systemes hyperboliques: Methodes et resultats qualitatifs". (Nonlinear oscillations of hyperbolic systems: Methods and qualitative results). (French) Ann. Inst. Henri Poincare, Anal. Non Lineaire 8, No.3/4, 351-417 (1991).

[17] D. Serre, "Oscillations non-linéaires de haute fréquence. Dim = 1", Nonlinear PDEs and their applications. Collège de France Seminar XII (1994).

[18] C. Cercignani, "The Boltzmann equation and its applications", Springer-Verlag, New-York, 1988.